



Potassium Map from Chang'E-2 Constraints the Impact of Crisium and Orientale Basin on the Moon

Meng-Hua Zhu^{1,2}, Jin Chang², Tao Ma², Wing-Huen Ip^{1,3}, WenZhe Fa⁴, Jian Wu², MingSheng Cai², YiZhong Gong², YiMing Hu², AoAo Xu¹ & ZeSheng Tang¹

¹Space Science Institute, Macau University of Science and Technology, Taipa, Macau, ²Purple Mountain Observatory, Nanjing 210008, China, ³Institutes of Astronomy and Space Science, National Central University, Taoyuan 32001, Taiwan, ⁴Institute of Remote Sensing and Geographical Information System, Peking University, Beijing 100871, China.

SUBJECT AREAS:
EARTH AND
ENVIRONMENTAL
SCIENCES
PLANETARY SCIENCE
INNER PLANETS
PHYSICAL SCIENCES

Received
20 November 2012

Accepted
25 March 2013

Published
8 April 2013

Correspondence and
requests for materials
should be addressed to
M.-H.Z. (mhzhu@must.
edu.mo)

KREEP materials were thought to be last crystallized at the lunar crust and mantle boundary. Impact cratering and volcanism are mainly responsible for their distributions on the lunar surface. Therefore, observation of global KREEP materials and investigation of distributions in the areas of large basins are of critical importance to understand the geologic history of the Moon. Here we report the new global potassium distribution on the Moon detected by Chang'E-2 Gamma-ray Spectrometer. We found that our new measurements are in general agreement with previous observation. A new finding and an important difference is that relatively higher K abundances in the Mare Crisium and Mare Orientale than their surrounding rims were detected for the first time. In light of our observations in these two areas, we propose that Crisium and Orientale basin-forming impact events may have penetrated to the lower crust and excavate the deeper materials to the lunar surface.

In the Lunar Magma Ocean (LMO) hypotheses¹, KREEP materials are proposed to lie between the mafic mantle and plagioclase crust in the process of compositional crystallization. Their presence on the lunar surface is the end product of a series of evolutionary processes that have changed the surface features of the Moon². In light of LMO hypotheses and the general impact cratering theory³, impact events penetrating through the crust should excavate the KREEP materials on the lunar surface. Therefore, observation of the global KREEP material on the Moon and the investigation of KREEP material in the areas of large basins are of critical importance to understand the formation of such a magma ocean and constrain the depth of the huge impact events.

In the past few years, several spacecraft with improved compositional remote sensing instruments were sent into the orbits around the Moon and large quantities of valuable data have been obtained. Chang'E-2 spacecraft, the second lunar probe of China, was launched on 1 October 2010, and inserted into a circular orbit of 100 km altitude on 15 October 2010. It carried a suite of remote sensing and plasma instruments. Here we report the results from the gamma ray spectrometer during its 178-days measurements and their new implications on the impact depth of the Crisium and of Orientale basin, respectively.

CE-2 GRS is the first gamma ray spectrometer that used large LaBr₃ crystal as the main detector to measure gamma rays emitted from the Moon within the energy region from 0.3-MeV to 9-MeV^{4,5}. The energy resolution of the flight model is ~ 5% full width at half maximum at 662 keV, which is about two times better than LPGRS⁶. Since CE-2 GRS was designed to be mounted inside the spacecraft, a big well-shape CsI(Tl) crystal was employed in anticoincidence with the main crystal to suppress the Compton effects and the background gamma rays from the spacecraft materials generated by Galactic Cosmic Rays (GCRs). Gamma rays emitted from the lunar surface are mainly from natural radioactive elemental (e.g., U, Th, K) decay effects and major elemental (e.g., Si, O, Fe, Ti, Mg, Al, Ca) excitation from interactions with incident GCRs⁷. Gamma rays entering the main crystal were recorded by the CE-2 GRS with a cadence of 3 second in the 512-channel spectrum.

More than 25 full energy peaks could be identified in CE-2 GRS spectra corresponding to different elements on the lunar surface (Fig. 1). But owing to the limitation of intrinsic energy resolution of the scintillation detector, many spectral peaks contain contributions from two or more elements. The strongest peak around 1.46 MeV is a combination of lines resulting mainly from the K line at 1.46 MeV and LaBr₃ self-activity because of the ¹³⁸La decay (1.436 MeV + 32 keV)⁸ that contributes about 85% of the corresponding gamma-ray intensity.

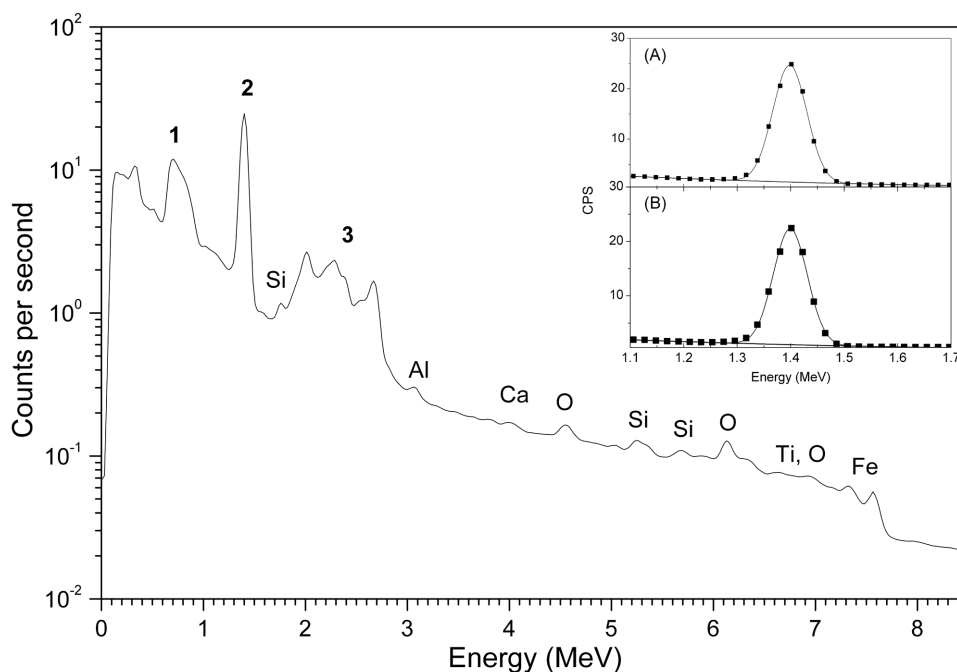


Figure 1 | Chang'E-2 gamma-ray spectrum plotted as counts per second (cps) of the whole Moon versus energy for its 178-days measurements with 100 km altitude. The major peaks are labeled. The spectrum below 2.7 MeV are mainly contributed by the self-activities from LaBr₃ crystal: natural ¹³⁸La is primarily responsible for the spectrum below 1.7 MeV while ²²⁷Ac decay chain generates alpha emitters between 1.7 and 2.7 MeV, as label 3. K line (1.46 MeV) is partly contributed to the sum peak as Label 2 with the ¹³⁸La decay to ¹³⁸Ba (1.436 MeV + 32 keV) of the LaBr₃ crystal; label 1 is the sum peak of elements from the Moon, and crystal beta decay of ¹³⁸La (789 keV) to ¹³⁸Ce. The inset figures are the fitting results of the energy region around 1.46 MeV. (A) The orbital spectrum and its fitting result. (B) The cruise spectrum and its fitting result.

Corrections of gain, solid angle, and cosmic ray variation have been carried out to CE-2 GRS measurements. The spatial resolution of CE-2 GRS is about 150 km in its 100 km working orbit, but in this work, all the corrected spectra are binned into equal-area pixels about 60 km × 60 km on the Moon. In our calculation we assumed gamma rays emitted from LaBr₃ self-activity decay are constant in the whole mission, the spectra measured in the cruise period could therefore be used as the background. The net ⁴⁰K gamma-rays emanating from the Moon in each pixel are obtained by calculating the peak fitting difference between binned spectra and the cruise spectrum (see inset of Fig. 1). Then all the net ⁴⁰K count rates from 11306 pixels were compared to count rates in the detector derived from the calculated surfaced gamma-ray fluxes to determine the abundance^{7,9,10}.

Results

The K distribution from CE-2 GRS (Fig. 2) is in general agreement with Lunar Prospector^{9,11,12}, Kaguya¹⁰, and Chang'E-1 measurements¹³. The global average abundance is 620 ± 615 ppm with the upper limit of 3240 ppm, which is lower than the LP value of 755 ± 740 ppm with the upper limit of 4360 ppm⁹. The Procellarum KREEP Terrane (PKT)¹⁴ has an average value of 1768 ± 530 ppm, comparing to 2004 ± 708 ppm determined by LPGRS. In the South Pole-Aitken (SPA) basin, the abundance ranges from 500 ppm to 1350 ppm with an average value of 615 ± 235 ppm, which is also lower than the LP measurements of 765 ± 320 ppm. Different from the PKT and SPA basin, lunar highlands is depleted in the K with the abundance being less than 500 ppm according to the CE-2 GRS observations. This is consistent with LP measurements⁹.

Mare basins on the nearside, such as Serenitatis, Tranquillitatis, Fecunditatis, and Crisium, have lower K abundance than mare regions. But after careful examination of the CE-2 GRS data, we found that the abundance within the Crisium impact basin is clearly higher than its surrounding highlands (Fig. 3a–b). This is inconsistent with previous LP results (Fig. 3c), which indicates that there is no

distinct difference between the K abundance of Mare Crisium and that of its surrounding¹¹.

Discussion

The Crisium basin is a Nectarian-age multi-ring impact structure on the eastern nearside of the Moon. Its interior is covered by mare basalt from a protracted period of volcanism over 0.8 Ga¹⁵. The abundance in its inner mare basalt ranges from 430 ppm to 840 ppm with an average value of 600 ± 100 ppm. On the other hand, the K abundance in the surrounding highlands is lower than 480 ppm with an average value of 290 ± 105 ppm. Because the southwest highlands is thought to be covered with ancient mare deposits¹⁶, not with ejecta from the Crisium basin, the abundance in its northeast highlands thus represents the true value of the ejecta for estimating the average value here (Fig. 3b). The highest K abundance in the Picard crater (14.6°N, 54.7°E) indicates the subjacent material has K abundance about 3 times (900 ppm) higher than highlands deposits surrounding the Crisium basin.

There is a long standing question concerning the origin of material excavated by the Crisium impact event^{16,17}. Some studies indicated that the Crisium impact event only excavated the upper or middle crustal material with a depth of about 40 km¹⁶ while others preferred that the impact event might have excavated mantle material¹⁷. According to recent observations of olivine sites around the Crisium basin¹⁷, the scenario that impact event only excavate upper or middle crustal material is probably excluded because olivine is a significant component associated with lunar mantle or Mg-rich plutons in lower crust¹⁸. Furthermore, if the Crisium impact event did penetrate through the crust and KREEP layer, exposing the upper mantle, KREEP (e.g., K here) and mafic materials should be found at its rim in light of the general impact cratering theory³, deep material will be spread around the near rim. However, higher K signal is not observed in Crisium rim and its basin terrain by CE-2 GRS, FeO is also found as lower as 2–4 wt.% in these areas¹⁹.

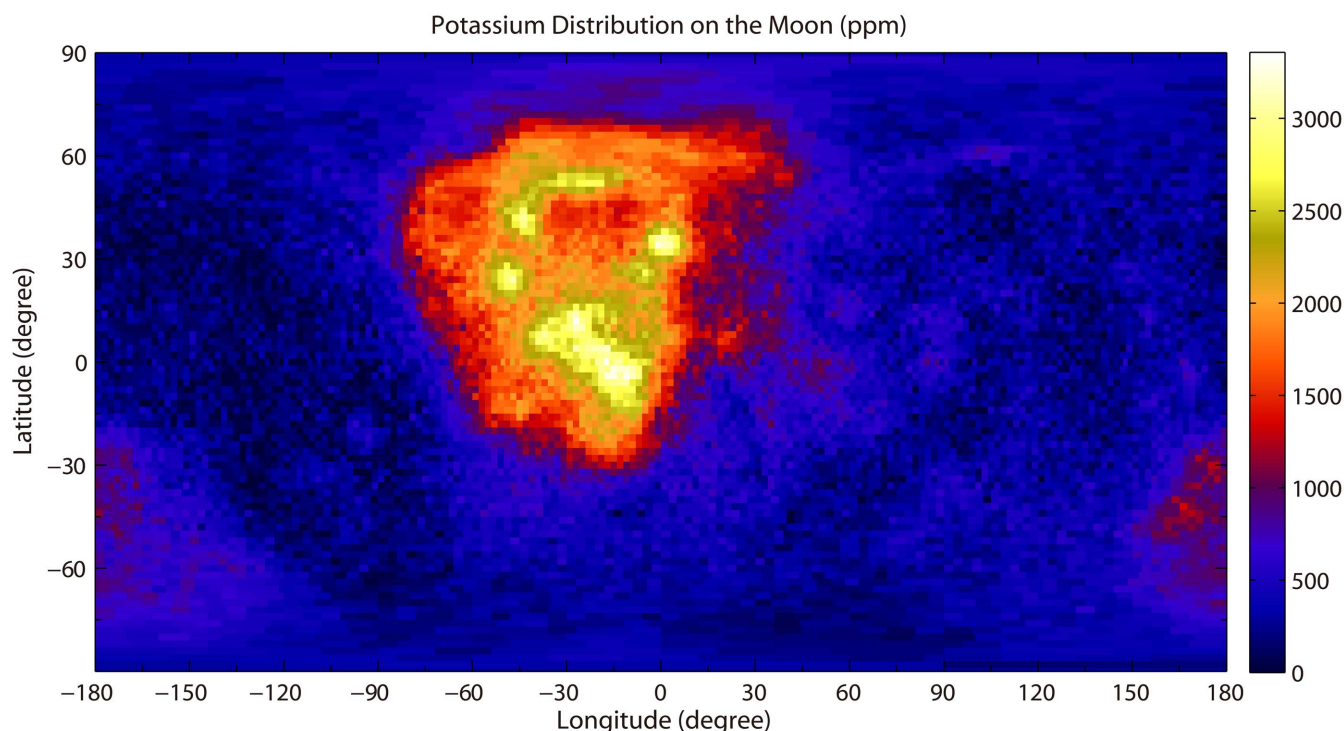


Figure 2 | The global K abundance (unit: ppm) of the Moon from CE-2 GRS 178-days measurements. All the data are binned into quasi-equals $2^\circ \times 2^\circ$ pixels in the equator and displayed in a cylindrical projection.

On the basis of our observation and previous results^{16,17,19}, we prefer the scenario that the Crisium impact event only penetrated to the plutonic lithosphere resulting from the magmatic intrusion into the lower crust. The magmatic intrusion, which is enriched in the PKT, is the hybrid source with low-density Mg-rich olivine at the base crust resulting from the overturn of the early mantle cumulate, KREEP, and crustal anorthosite²⁰. While the Crisium impact event penetrated through the crust, to the upper boundary of the magmatic intrusion, the deepest materials would be ejected to the surrounding rim area. The redistribution of excavated material resulted in the lower K and FeO in the highlands¹⁹ bounding the basin and is in agreement with the observations of olivine exposure on the basin rim¹⁷. The constraint of impact to the upper boundary of the magmatic intrusion is consistent with the higher K abundance in sub-jacent highlands material covered by mare basalt as detected in the Picard crater, and is also consistent with the non-zero crustal thickness in the Crisium basin²¹. The big basin formation impact excavated tremendous volume material and formed a thinner crust with fracturing underlying lithosphere²² in the Crisium area. Owing to the density difference between lower crust and partly melted magma, the buoyancy contrast²³ enabled the eruption of basalts at the Crisium basin. The partly melted magma is from the Moon's deep interior and produced by slowly heating up from the decay of radioactive elements. This supports the observations of higher K abundance (about 600 ppm) and very higher FeO contents¹⁹ (up to 20 wt.% for areas of the central areas) in the mare basalts covered in the Crisium basin. Located near the PKT region and consistent K abundance with mare basalts in the PKT boundary, high-heat production by radioactive decay is suggested to be responsible to the long duration of volcanic extrusions at the Crisium basin¹⁶.

Similar characteristics are also found in the Orientale basin (Fig. 4a–d), the youngest multi-ring basin on the Moon²⁴. CE-2 GRS shows that the central areas (5–6 pixels in diameter with each pixel of ~ 60 km) of the Orientale basin corresponding to the Mare Orientale, the largest mare deposit (~ 320 km in diameter) in the basin, has obviously high K abundance with the average of $360 \pm$

115 ppm (Fig. 4b). This value is about a factor of two higher than the surrounding areas, including the Montes Rook Formation (MRF) occurring mostly between the edge of the Inner Depression (ID) and Cordillera Ring (CR), and Hevelius Formation (HF) lying outside the CR. The MRF, consisting of smooth plains and corrugated deposits, has K abundance of 115 ± 95 ppm (Fig. 4b), which is only one-third of that in the Mare Orientale. Most areas of HF, which represent the radial ejecta deposits from the Orientale basin, have an average abundance a little higher (about 80 ppm) than the deposits in MRF, except two areas located at the southwest (K-1) and northwest (K-2) portion of the basin (Fig. 4d). These two areas, related to the well-preserved ejecta units in MRF (part of K-1) and HF²⁵, have abundance of 270 ± 80 ppm (K-1) and 255 ± 90 ppm (K-2), respectively. Because turbulent impact modification after Orientale impact event has less influence on these two areas²⁶, the K abundances in these two areas therefore represent the original value of excavated ejecta from the basin-forming impact.

Assuming the Out Rook Ring is the closest approximation to the basin excavation cavity, CR is believed to have been formed by the inward collapse at the edge of structural uplift along the basin of the displaced zone²⁵. MRF therefore represents the modification of rim ejecta and the mixture with the upper crust, which could be consistent with the similar K abundance in HF and MRF. The relative higher K abundance (about 80 ppm) in HF implies that the deeper material excavated by the impact event has relatively higher K abundance. The LMO scenario proposes that the KREEP layer lies between the anorthositic lunar crust and mafic cumulated mantle in the long-time compositional differentiation¹. Therefore, in contrast to previous works²⁷ which suggested that Orientale impact event excavated only to the upper half of the lunar crust in its target region with the depth of 40–50 km, we prefer that the Orientale impact event penetrated into a source of radioactive-rich material at the lower crust. This scenario supports the lower FeO (2–4 wt.%)¹⁹ in the surrounding of the Orientale basin and is also consistent with the estimated crustal thickness in this area²¹. This scenario is also consistent with the enrichment of

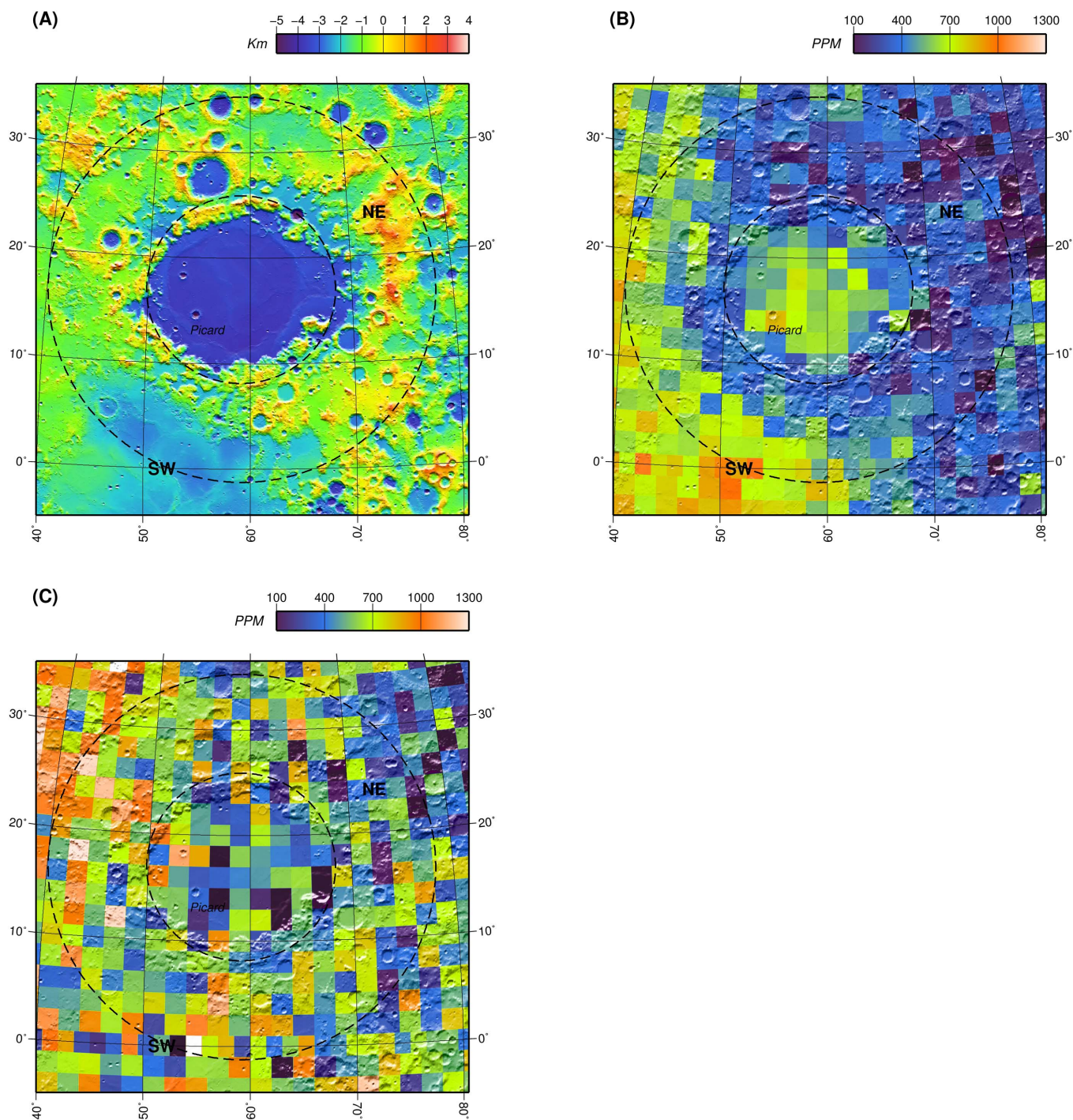


Figure 3 | Surface topography and K distributions of the 550-km-diameter Crisium Basin. All the maps are displayed in a Lambert azimuthal equal-area projection superimposed on the shaded lunar surface relief. Two circles represent the proposed rims with diameter of 300 km and 700 km. NE - northeast highlands of Crisium basin; SW - southwest of Crisium basin that covered by ancient mare basalt. Picard - Picard crater with 30 km in diameter. (A) the topographic elevation of the Crisium basin from Lunar Orbiter Laser Altimeter³². (B) K abundance of the Crisium Basin measured by CE-2 GRS with data binned into quasi-equal $2^\circ \times 2^\circ$ pixels. (C) K abundance of the Crisium basin measured by LPGRS⁹.

low-Ca pyroxene in the central peaks of the Mauser crater, a post-Orientele crater with 55 km diameter in the interior depression of the Orientele basin, which is thought to be sampling the noritic lower crust²⁶.

The internal accumulation of radiogenic heat sources causing partial melting of the mantle is the basic postulation for the formation of mare basalt²⁸. The details of the generation, ascent and eruption of the mare basalts in the Orientele basin need further investigations, but the similar K abundance in the Mare Orientele to the nearside

mare basalts, especially to the boundary of PKT, suggests that mare deposits within Orientele basin are similar in composition to nearside mare basalts²⁷. Furthermore, two areas with higher K abundance in the Mare Orientele definitely correspond to the eastern and north-western region of the inner depression covered by mare basalts, which have almost the identical age, $\sim 3.2\text{--}3.3\text{ Ga}$ ^{29,30}. The same concentration of FeO, TiO₂¹⁹, and K in these two areas supports the interpretation that the covered basalts in the center of Orientele basin are from single volcanic events^{29,31}.

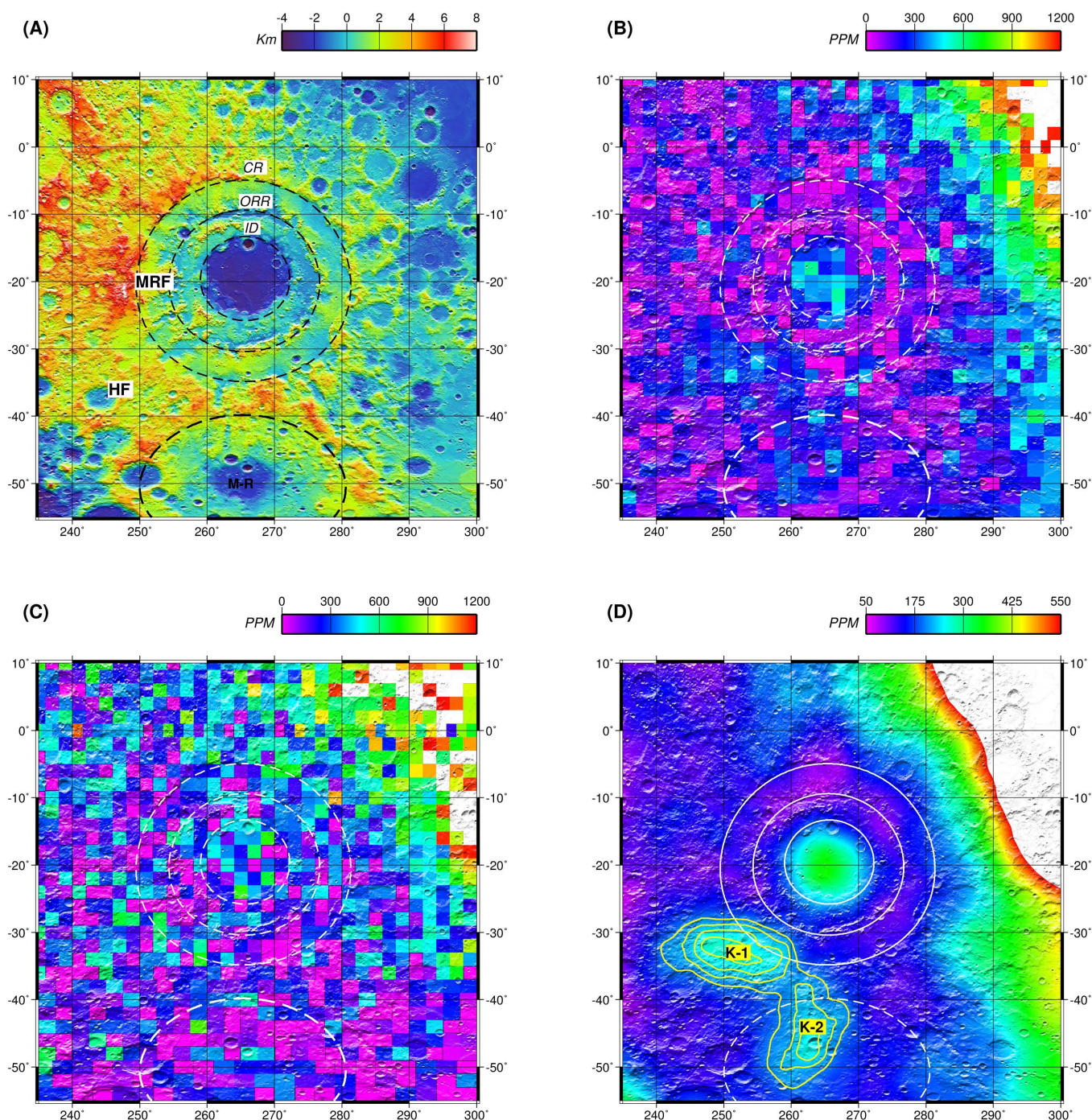


Figure 4 | Orientale Basin and the K distribution from CE-2 GRS and LPGRS in cylindrical equidistant projection superimposed on the shaded lunar surface relief. (A) the topographic elevation of the Orientale basin from Lunar Orbiter Laser Altimeter³² with the black circles represent the rings of the Orientale basin (CR, ORR), but the Inner Rook Ring is not shown here; CR - Cordillera Ring; ORR - Out Rook Ring; ID - Inner Depression; MRF - Montes Rook Formation; HF - Hevelius Formation; M-R - Mendel-Rydberg basin. (B) K abundance in the Orientale Basin measured by CE-2 GRS with data binned into quasi-equal $2^\circ \times 2^\circ$ pixels. (C) K distribution in the Orientale basin measured by LPGRS⁹. (D) the smoothed K distribution from CE-2 GRS measurements; K-1/2 represent two areas with relatively higher K Abundances outside the CR. The yellow lines represent the contours of K abundance in K-1/2 area.

Methods

All raw data received from the spacecraft were converted to time series gamma ray spectra that were used to derive elemental maps. However, in order to ensure the correctness of spectral analysis, mapping, and abundance calculations, data selection was carried out at first. We eliminated the data which have bad sync words, bad check sums, and off-limit values. The measurements during solar energetic particle event were also excluded. In this work, the energetic proton data taken from the Earth orbiting GOES satellites³³ were used to identify the solar energetic particle events.

Three major corrections to the time series data were made for the variations of gain, galactic cosmic ray, and solid angle before analyzing the spectra. To monitor

the gain changes, we calculated the peak positions of two strong peaks (0.511 MeV, 7.60 MeV) for every 15-min and every 3-hour interval. The time series data were then corrected according to the gain and offset values for each 3-hour and 15-min interval³⁴. The time-varying galactic cosmic ray flux was monitored by measuring the counting rate of oxygen gamma ray line (6.13 MeV) for all latitudes poleward of $+85^\circ$. In order to apply the galactic cosmic ray correction, the 6.13 MeV counting rate were smoothed and normalized to the counting rate seen at the beginning of the orbital mission. All spectra were then divided by this normalized flux for the correction of the galactic cosmic ray variations³⁴. In addition, all spectra were normalized to a spacecraft height of



100 km to normalize the variations of solid angle seen by the detector due to height variation from 85 to 125 km.

All corrected spectra were binned into approximately equal-area pixels about 60 km × 60 km by using their latitude and longitude positions at the times they were taken. Gamma-ray spectra were accumulated in each pixel to present the spectrum measured from such area. To calculate the K counting rate in each pixel, the integrated area beneath K peak should be determined. In this work, peak fitting method (Gaussian shaped, linear background line) was used to determine K peak area in each pixel. Since the peak around 1.46 MeV is a combination of lines resulting mainly from the K line at 1.46 MeV and LaBr₃ self-activity because of the ¹³⁸La decay (1.436 MeV + 32 keV)⁸, the contribution of LaBr₃ self-activity should be eliminated from each calculation. We assumed that gamma rays emitted from LaBr₃ self-activity decay were constant in the whole mission. The peak area estimated from the accumulated spectrum in the cruise period was used to eliminate the contribution of LaBr₃ self-activity. The net ⁴⁰K gamma-rays emanating from the Moon in each pixel were obtained by calculating the area difference between binned spectra and the cruise spectrum.

- Warren, P. H. The magma ocean concept and lunar evolution. *An. Rev. Earth Planet. Sci.* **13**, 201–240 (1985).
- Hiesinger, H. & Head, J. W. New views of lunar geosciences: An introduction and overview. *Rev. Mineral. Geochem.* **60**, 1–81 (2006).
- Melosh, H. J. *Impact Cratering*, (Oxford University Press, 1989).
- Ma, T. *et al.* Gamma-ray spectrometer onboard Chang'E-2. *Acta Astronomica Sinica* **54**, 1–9 (2013).
- Zhu, M. H. *et al.* The measurements of Gamma-ray spectrometer from China's Chang'E-1/2 spacecrafts (abstract). *39th COSPAR Scientific Assembly* (2012).
- Feldman, W. C. *et al.* The lunar prospector gamma ray and neutron spectrometers. *Nucl. Instr. Meth Phys. Res.* **422**, 562–566 (1999).
- Reedy, R. C. Expected gamma ray emission spectra from the lunar surface as a function of chemical composition. *J. Geophys. Res.* **78**, 5847–5866 (1973).
- Kernan, W. J. Self-activity in lanthanum halides. *IEEE Trans. Nucl. Sci.* **53**, 395–400 (2006).
- Prettyman, T. H. *et al.* Elemental composition of the lunar surface: analysis of gamma ray spectroscopy data from lunar prospector. *J. Geophys. Res.* **111**, E12007 (2006).
- Kobayashi, S. *et al.* Determining the absolute abundances of natural radioactive elements on the lunar surface by the Kaguya gamma-ray spectrometer. *Space Sci. Rev.* **154**, 193–218 (2010).
- Lawrence, D. J. *et al.* Global elemental maps of the Moon: the lunar prospector gamma-ray spectrometer. *Science* **281**, 1484–1489 (1998).
- Lawrence, D. J. *et al.* Thorium abundances on the lunar surface. *J. Geophys. Res.* **105**, 20,307–20,331 (2000).
- Zhu, M. H., Ma, T. & Chang, J. Chang'E-1 gamma ray spectrometer and preliminary radioactive results on the lunar surface. *Planet. Space. Sci.* **58**, 1547–1554 (2010).
- Jolliff, B. L. *et al.* Major lunar crustal terrain: surface expressions and crust-mantle origins. *J. Geophys. Res.* **105**, 4197–4216 (2000).
- Fernandes, V. A. & Burgess, R. Volcanism in Mare Fecunditatis and Mare Crisium: Ar-Ar age studies. *Geochim. Cosmochim. Acta* **69**, 4919–4934 (2005).
- Schultz, P. H. & Spudis, P. D. Evidence for ancient mare volcanism. *Proc. Lunar Planet. Sci. Conf.* **10**, 2899–2918 (1979).
- Yamamoto, S. *et al.* Possible mantle origin of olivine around lunar impact basins detected by SELENE. *Nat. Geosci.* **3**, 533–536 (2010).
- Pieters, C. M. & Wilhelms, D. E. Origin of olivine at Copernicus. *J. Geophys. Res.* **90**, C415–C420 (1985).
- Bussey, D. B. & Spudis, P. D. Compositional studies of the Orientale, Humorum, Nectaris, and Crisium lunar basins. *J. Geophys. Res.* **105**, 4235–4243 (2000).
- Elardo, S. M., Draper, D. S. & Shearer, Jr. C. K. Lunar Magma Ocean crystallization revisited: Bulk composition, early cumulate mineralogy, and the source regions of the highlands Mg-suite. *Geochim. Cosmochim. Acta* **75**, 3024–3045 (2011).
- Ishihara, Y. *et al.* Crustal thickness of the Moon: implications for farside basin structures. *Geophys. Res. Lett.* **36**, L19202 (2009).
- Wilhelms, D. E. *The Geologic History of the Moon* (U.S. Geological Survey Professional Paper no. 1348, Washington, DC, 1987).
- Wieczorek, M. A., Zuber, M. T. & Phillips, R. J. The role of magma buoyancy on the eruption of lunar basalts. *Earth Planet. Sci. Lett.* **185**, 71–83 (2001).
- Scott, D. H. *et al.* U.S. Geol. Survey Misc. Geol. Inv. Map I-1034 (1977).
- Head, J. W. *et al.* Global distribution of large lunar craters: implications for resurfacing and impactor populations. *Science* **329**, 1504–1507 (2010).
- Head, J. W. *et al.* Lunar impact basins: new data for the western limb and farside (Orientale and South Pole-Aitken Basins) from the first Galileo flyby. *J. Geophys. Res.* **98**, 17,149–17,181 (1993).
- Spudis, R. D., Hawke, B. R. & Lucey, P. Composition of Orientale basin deposits and implications for the lunar basin-forming process. *J. Geophys. Res.* **89**, C197–C210 (1984).
- Shearer, C. K. *et al.* Thermal and magmatic evolution of the Moon. *Rev. Mineral. Geochem.* **60**, 365–518 (2006).
- Whitten, J. *et al.* Lunar mare deposits associated with the Orientale impact basin: new insights into mineralogy, history, mode of emplacement, and relation to Orientale basin evolution from Moon Mineralogy Mapper data from Chandrayaan-1. *J. Geophys. Res.* **116**, E00G09 (2011).
- Cho, Y., Morata, T., Haruyama, J., Yasui, M., Hirata, N. & Sugita, S. Young mare volcanism in the Orientale region contemporary with the Procellarum KREEP Terrane (PKT) volcanism peak period ~ 2 billion years ago. *Geophys. Res. Lett.* **39**, L11203 (2012).
- Yingst, R. A. & Head, J. W. Volumes of lunar lava ponds in South Pole-Aitken and Orientale basins: Implications for eruption conditions, transport mechanisms and magma source regions. *J. Geophys. Res.* **102**, 10,909–10,931 (1997).
- Smith, D. E. *et al.* Initial observations from the Lunar Orbiter Laser Altimeter (LOLA). *Geophys. Res. Lett.* **37**, L18204 (2010).
- <http://www.swpc.noaa.gov>.
- Lawrence, D. J., Maurice, S. & Feldman, W. C. Gamma-ray measurements from Lunar Prospector: Time series data reduction for the gamma-ray spectrometer. *J. Geophys. Res.* **109**, E07S05 (2004).

Acknowledgements

The authors thank Chang'E-2 project team members for their work. This research was supported by the Science and Technology Development Fund of Macau (004/2011/A1; 048/2012/A2) and National Natural Science Foundation of China (11103089).

Author contributions

M.Z. drafted the manuscript. J.C. is the principle investigator of the GRS, and contributed to the data process and analysis with M.Z. W.I. and W.F. contributed scientific interpretations with M.Z. J.C., T.M., J.W., Y.G., M.C. and Y.H. were responsible for development and operation of the GRS system. All of the authors, including A.X. and Z.T. discussed and provided significant comments on the results and manuscript.

Additional information

Competing financial interests: The authors declare no competing financial interests.

License: This work is licensed under a Creative Commons Attribution-NonCommercial-NoDerivs 3.0 Unported License. To view a copy of this license, visit <http://creativecommons.org/licenses/by-nc-nd/3.0>

How to cite this article: Zhu, M. *et al.* Potassium Map from Chang'E-2 Constraints the Impact of Crisium and Orientale Basin on the Moon. *Sci. Rep.* **3**, 1611; DOI:10.1038/srep01611 (2013).